

The Minimum-Mass Extrasolar Nebula: *In-Situ* Formation of Close-In Super-Earths

Eugene Chiang¹[★] and Gregory Laughlin²[★]

¹*Departments of Astronomy and of Earth and Planetary Science, University of California, Berkeley, Hearst Field Annex B-20, Berkeley CA 94720-3411, USA*

²*Department of Astronomy and Astrophysics, UCO/Lick Observatory, University of California, Santa Cruz, Santa Cruz, CA 95064, USA*

Submitted: 21 February 2022

ABSTRACT

Close-in super-Earths, with radii $R \approx 2\text{--}5R_{\oplus}$ and orbital periods $P < 100$ d, orbit more than half, and perhaps nearly all Sun-like stars in the universe. We use this omnipresent population to construct the minimum-mass extrasolar nebula (MMEN), the circumstellar disk of solar-composition solids and gas from which such planets formed, if they formed near their current locations and did not migrate. In a series of back-of-the-envelope calculations, we demonstrate how *in-situ* formation in the MMEN is fast, efficient, and can reproduce many of the observed properties of close-in super-Earths, including their gas-to-rock fractions. Testable predictions are discussed.

Key words: planets and satellites: general – planets and satellites: atmospheres – planets and satellites: composition – planets and satellites: formation – protoplanetary discs

1 INTRODUCTION

The Solar System has provided, and continues to provide, the *de facto* template for most discussions of planet formation. But with a multitude of extrasolar worlds now known, with masses approaching those of our terrestrial planets, we can ask whether the Solar System’s orbital architecture is the norm — or whether a new template is needed.

1.1 Close-in super-Earths are ubiquitous

The HARPS (High Accuracy Radial-Velocity Planet Searcher) project reported that $> 50\%$ of chromospherically quiet, main-sequence dwarf stars in the Solar neighborhood are accompanied by planets with masses $M \sin i \lesssim 30 M_{\oplus}$ and orbital periods $P < 100$ days — hereafter “close-in super-Earths” (Mayor et al. 2011). Such a startlingly large occurrence rate appears consistent with the latest results of the *Kepler* mission, as we now argue. Batalha et al. (2012) used *Kepler* to survey $N_{*,\text{total}} = 1.56 \times 10^5$ stars — almost all main-sequence solar-type dwarfs (G. Marcy 2012, personal communication). Define:

- $\mathcal{F}_{\text{intrinsic}}$ to be the fraction of *Kepler* dwarfs that host at least one close-in super-Earth with radius $R > 2R_{\oplus}$ and $P < 100$ days;
- $\mathcal{F}_{\text{detect}}$ to be the fraction of systems with close-in super-Earths whose transit light curves achieve the mandated detection threshold

to be listed as candidates in the Batalha et al. (2012) catalog (i.e., among the subset of *Kepler* dwarfs which actually do host close-in super-Earths, $1 - \mathcal{F}_{\text{detect}}$ is the fraction that are missing from the catalog);

- $\mathcal{F}_{\text{transit}} \approx 2.5\%$ to be the geometric probability of transit averaged over a distribution of planets for which $dN/d \log P \propto P^{1/2}$ between $P = 7$ and 100 days (Youdin 2011).¹

Batalha et al. (2012) reported that $N_* = 1.8 \times 10^3$ individual stars harbor $\sim 2.3 \times 10^3$ planet candidates — more than 80% of which have radii $R < 5 R_{\oplus}$. *In toto* we have

$$\mathcal{F}_{\text{intrinsic}} \mathcal{F}_{\text{detect}} \mathcal{F}_{\text{transit}} N_{*,\text{total}} = N_* \quad (1)$$

or

$$\mathcal{F}_{\text{intrinsic}} \approx 0.5 \left(\frac{1}{\mathcal{F}_{\text{detect}}} \right) \left(\frac{N_*}{1.8 \times 10^3} \right) \left(\frac{1.56 \times 10^5}{N_{*,\text{total}}} \right) \left(\frac{0.025}{\mathcal{F}_{\text{transit}}} \right) \quad (2)$$

which implies that $\mathcal{F}_{\text{intrinsic}} \gtrsim 50\%$, in accord with the occurrence rate calculated by Mayor et al. (2011). Figueira et al. (2012) performed a more careful consistency analysis between the results of the HARPS and *Kepler* surveys, and found that the two exoplanet

¹ The best-fit slope of the period distribution of Youdin (2011) derives from only about half of the planet candidates found in the Batalha et al. (2012) catalog, and moreover applies only up to $P = 50$ days. Fortunately, our calculation of the average $\mathcal{F}_{\text{transit}}$ is not sensitive to the exact slope of the period distribution as long as it is fairly flat. For example, $dN/d \log P \propto P^0$ yields $\mathcal{F}_{\text{transit}} = 3.0\%$.

[★] e-mail: echiang@astro.berkeley.edu, laugh@ucolick.org

populations can be reconciled — and the large number of multiple-transiting systems accounted for — if planet-planet mutual inclinations are less than ~ 1 degree.²

It seems clear that our Solar System — which contains no planet interior to Mercury’s $P = 88$ day orbit — did not participate in a major if not the dominant mode of planet formation in the Galaxy.

1.2 Close-in super-Earths are a distinct population with possible ties to giant planet satellites

Aside from being commonplace, close-in super-Earths form a distinct population in the space of $\log(M/M_*)$ and $\log P$, where M_* is the host primary mass. In Figure 1, super-Earths are well separated from hot Jupiters, and are also distinct from Jovian-mass planets with $P > 100$ days — the latter having generally eccentric orbits (Zakamska et al. 2011). Jupiter lies on the fringe of the exo-Jupiter distribution, and its position on the edge may be real. Arguably, the Doppler surveys have had more than adequate time baseline and precision to uncover an abundance of true-Jupiter analogs if they existed (Burt et al. 2013, in preparation, will present a comprehensive analysis of radial velocity measurements from the Keck-I iodine cell spanning the years 1998–2012).

The super-Earth population is characterized by (i) orbital periods ranging from days to weeks, (ii) mass ratios $M/M_* \sim 10^{-4.5}$, and (iii) orbits that are co-planar to within a few degrees (e.g., Fang & Margot 2012; Fabrycky et al. 2012; Tremaine & Dong 2012). All these properties are reminiscent of the regular satellite systems of Solar System giant planets. The fact that Jupiter, Saturn, and Uranus³ all possess broadly similar satellite systems indicates that the satellite formation process is robust — just as robust as the formation process for close-in super-Earths, with which it may share more than a passing resemblance.

One difference between satellites and super-Earths is the propensity of the former to be found in mean-motion resonances. Tidal interactions with the host planet expand satellite orbits and drive convergent migration into resonances (Murray & Dermott 2000). In the case of close-in super-Earths, tidal changes to orbital semimajor axes are typically less dramatic. Nevertheless, tides may still shape super-Earth orbits in observable ways: tidal dissipation can damp orbital eccentricities and wedge near-resonant planets farther apart (Lithwick & Wu 2012; Batygin & Morbidelli 2012). This process may explain the observed excess of *Kepler* planet pairs just outside of resonance (Lissauer et al. 2011b; Fabrycky et al. 2012).

1.3 Migration vs. *in-situ* accretion

Giant planets with $P \ll 100$ days are commonly thought to have formed at distances of several AUs from their host stars, and then to have migrated to their current locations. The difficulty of forming hot Jupiters *in situ* is frequently acknowledged (e.g., Rafikov

2006). Migration has also been invoked to explain the close-in orbits of lower-mass super-Earths (e.g., Alibert et al. 2006; Schlaufman et al. 2009; Lopez et al. 2012). Although much of the work on orbital migration is well-motivated, we wonder how much stems from an insistence (perhaps only implicit) on using the Solar System — with its obvious lack of close-in planets — as a starting point for studies of planet formation.⁴ To what extent is our view still provincial, unduly colored by a naive interpretation of one system?

A popular mechanism for transporting planets inward is via gravitational torques exerted by parent disks (see Kley & Nelson 2012 for a review). At the moment, disk-driven migration seems too poorly understood to connect meaningfully with observations. Population synthesis models that include prescriptions for disk-driven migration fail to reproduce the observed statistics of planet occurrence at $P \lesssim 50$ days (Ida & Lin 2010; Howard et al. 2010; Howard et al. 2012, and references therein). Theoretical uncertainties include the effects of co-rotation resonances, disk thermodynamics (which can even cause planets to migrate outward; see, e.g., section 2.2 in Kley & Nelson 2012, and references therein), and the perennial mystery of the source of viscosity in protoplanetary disks. It seems premature to discuss how planets are transported in disks when we cannot reliably say how disk material itself is transported.

Planets that migrate smoothly and converge on one another can trap themselves into mean-motion resonances, but most planetary systems do not exhibit such resonances. Period ratios of multi-planet systems discovered by *Kepler* appear to be largely random, aside from a small preponderance of ratios just greater than 3:2 and 2:1 that can be attributed to a modest amount of differential tidal decay (Lissauer et al. 2011b; Fabrycky et al. 2012; Lithwick & Wu 2012; Batygin & Morbidelli 2012). Among more massive giant planets discovered by the radial velocity method, Wright et al. (2011b) show that the occurrence rate of period commensurabilities is greater than random, but is still only about 1 in 3 — and in most cases resonant libration cannot be confirmed. Even for Gliese 876 b and c — a pair of giant planets trapped deeply in a 2:1 resonance — the amount by which these planets migrated differentially could have been as small as $\sim 7\%$ (Lee & Peale 2002; see also Rivera et al. 2010).

Disk-driven migration is not the only means of migration. Gravitational torques can be supplied instead by additional planetary or even stellar companions. Hot Jupiters whose orbit normals are severely misaligned with the spin axes of their host stars seem most naturally explained by dynamical instabilities that can deliver giant planets onto high-eccentricity, high-inclination orbits. Such orbits can circularize by stellar tidal friction while retaining their large inclinations (for a general overview of the dynamics, see Wu & Lithwick 2011). Although inward transport nicely explains spin-misaligned hot Jupiters, we emphasize that hot Jupiters as a whole represent but a small fraction of the entire close-in population of planets — i.e., hot Jupiters, and the need for large-distance migration that they imply, may be the exception rather than the rule. The occurrence rate of hot Jupiters is only about $\sim 1\%$ (e.g., Mayor et

² Our equation (1) is strictly valid only for coplanar or single-planet systems. A transit survey alone cannot determine $F_{\text{intrinsic}}$ without assuming an inclination distribution for multi-planet systems (see, e.g., Tremaine & Dong 2012).

³ Presumably Neptune also once harbored a regular satellite system, which was destroyed when Triton was captured (Goldreich et al. 1989).

⁴ Migration may also have occurred in our Solar System, but arguably not to the dramatic extents imagined for close-in exoplanets. A classic and still viable scenario for the migration of giant planets in our primordial planetesimal disk posits that Jupiter migrated inward by a fraction of an AU while Neptune migrated outward from ~ 22 to 30 AU (Fernandez & Ip 1984; Malhotra 1993).

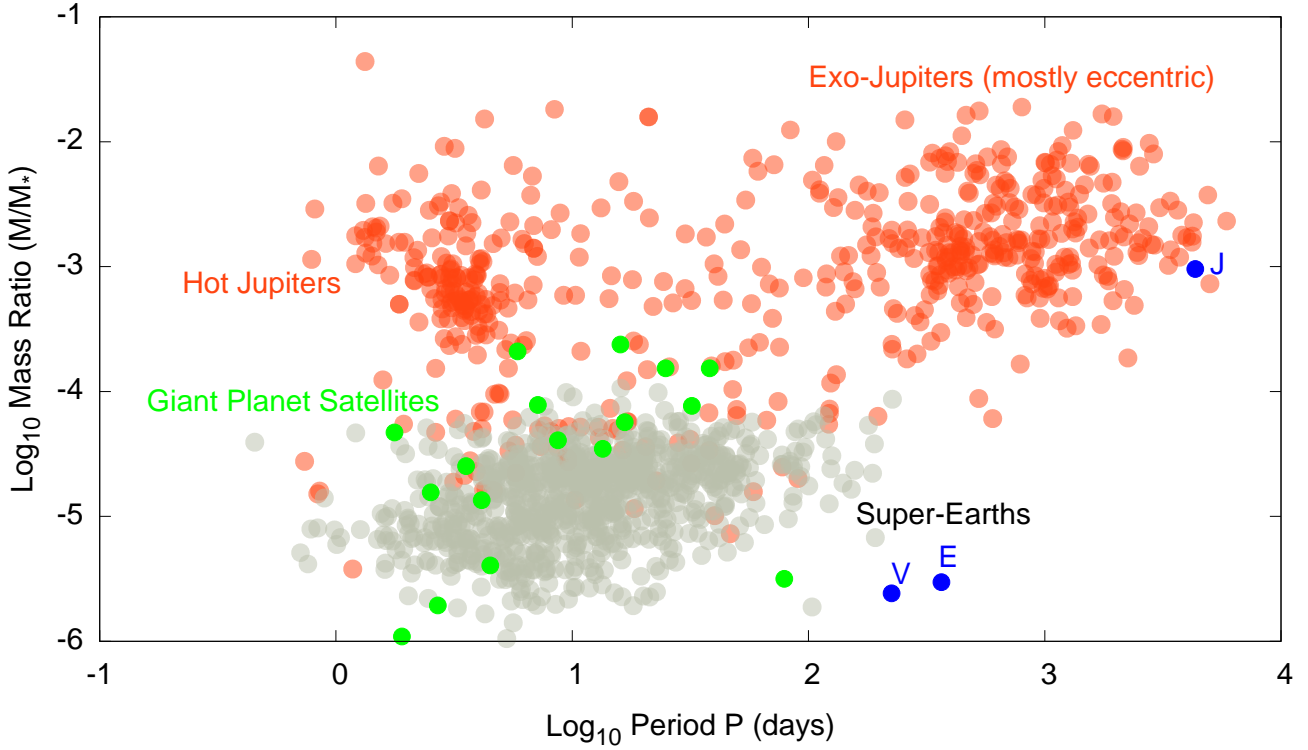


Figure 1. A “bird’s eye view” of published extrasolar planets. We argue in this paper that hot Jupiters and super-Earths have distinct formation histories: hot Jupiters may have formed among the main population of exo-Jupiters at long orbital periods and migrated inward, whereas super-Earths formed *in situ*. Hot Jupiters are a fringe population as they are found orbiting only $\mathcal{F}_{\text{intrinsic}} \approx 0.5\text{--}1\%$ of Sun-like stars. By contrast, close-in super-Earths abound, with $\mathcal{F}_{\text{intrinsic}} \gtrsim 50\%$. *Red circles:* Planets detected by the radial velocity method (either with or without photometric transits), taken from www.exoplanets.org on 07 Oct 2012 (see also Wright et al. 2011a). Planet masses are $M \sin i$. *Gray circles:* *Kepler* Objects of Interest (KOI) for which multiple KOIs are associated with a single target star. Radii, as reported in Batalha et al. (2012), are converted to masses by using $M/M_{\oplus} = (R/R_{\oplus})^{2.06}$, the best-fit power relation for planets in the Solar System (see §2.2 for alternative mass-radius relations). Only KOIs for which $R < 5R_{\oplus}$ are plotted. *Green circles:* Regular satellites of the Jovian planets in our Solar System. Mass ratios are those of satellites to their host planets. *Blue circles:* Jupiter, Earth and Venus.

al. 2011; Howard et al. 2012; from the Batalha et al. 2012 catalog we estimate an occurrence rate of 0.5%), in contrast to the order-unity occurrence rate of close-in super-Earths (§1.1). While migration of one kind or another may be necessary to explain the fringe population represented by hot and even warm Jupiters, the same may not be true for the majority of close-in planetary systems — particularly the ubiquitous super-Earths, lying as they do in a distinct region of parameter space (Figure 1).

Here we explore the possibility that long-distance orbital migration does not play a major role in the genesis of close-in super-Earths — that such worlds formed instead *in situ* from circumstellar disks of solids and gas extending interior to 0.5 AU. This idea is certainly not new; it is nothing more than an extension of the classical formation scenario for our Solar System’s terrestrial planets to distances inside Mercury’s orbit. Recent explorations of *in-situ* accretion include those by Raymond et al. (2008; see their Table 1 and Figure 1), Montgomery & Laughlin (2009), and Hansen & Murray (2012), and in many respects our work parallels theirs. In a similar vein, Ikoma & Hori (2012) calculated how close-in rocky cores accreted gas *in situ*, with specific application to the gas-laden super-Earths orbiting Kepler-11. Some of these papers still appealed to the transport of solids from regions beyond 0.5 AU: Hansen &

Murray (2012) invoked inward migration of planetesimals to furnish a massive enough reservoir of raw rocks to form super-Earths, and Ikoma & Hori (2012) assumed that the progenitor cores of the Kepler-11 planets migrated inward to their current locations.

1.4 Plan of this paper

As we have argued above, close-in super-Earths are not anomalous — they are the norm, and it is our Solar System that is the exception to the rule that the majority of main-sequence Sun-like stars harbor planets with $R > 2R_{\oplus}$ and $P < 100$ days. We compute from scratch a “minimum-mass extrasolar nebula” (MMEN) using the abundance of data from the *Kepler* mission (§2).⁵ How the MMEN can spawn close-in super-Earths *in situ* is explored through a series of back-of-the-envelope calculations that readers are encouraged to reproduce and/or challenge (§3). *In-situ* formation leads to a number of predictions that seem ripe for testing (§4).

⁵ An earlier attempt to compute the MMEN using Doppler-detected planets is made by Kuchner (2004).

2 MINIMUM-MASS EXTRASOLAR NEBULA (MMEN)

We construct the “minimum-mass extrasolar nebula” (MMEN): the solar-metallicity disk of gas and solids out of which the super-Earths uncovered by *Kepler* could have formed, if planet formation were 100% efficient and orbital migration were negligible. We employ the $N = 1925$ planet candidates with radii $R < 5R_\oplus$ and $P < 100$ days reported by Batalha et al. (2012) for the first 480 days of *Kepler* observations.

We idealize the *Kepler* planets as being composed of “solar composition solids”; in other words, we assume they are bulk chondritic and contain little H and He by mass. This assumption is compatible with models of planetary interiors that reproduce the observed radii and masses of close-in super-Earths. Models comprising gaseous H/He atmospheres overlying rocky cores are typically characterized by low ($\lesssim 20\%$) gas fractions by mass (e.g., Rogers & Seager 2010; Lissauer et al. 2011a; see also §3.3). Of course, merely knowing the radius and mass of a planet is not sufficient to uniquely constrain its bulk composition. In particular, worlds made predominantly of water are also possible (e.g., Lopez et al. 2012). In this paper, we discount water worlds on the grounds that water cannot condense *in situ* in the hot inner regions of protoplanetary disks (but see §3.7.3 for a way to create close-in water worlds in a less strict *in-situ* formation scenario).

Each of the *Kepler* planets is assigned a surface density

$$\sigma_{\text{solid},i} \equiv \frac{M_i}{2\pi a_i \Delta a_i} \equiv \frac{M_i}{2\pi a_i^2} \quad (3)$$

where $M_i = (R_i/R_\oplus)^{2.06} M_\oplus$ (the best-fit power-law mass-radius relation for the six Solar System planets bounded in mass by Mars and Saturn; Lissauer et al. 2011b), and $\Delta a_i = a_i = (P/\text{yr})^{2/3}$ AU is the semimajor axis computed by assuming the host star has mass $M_* = M_\odot$. For simplicity, we apply equation (3) without regard to whether a planet is solitary or is in a multi-planet system — and have checked that accounting for the relative spacings between planets when computing Δa in multi-planet systems does not significantly change the overall distribution of inferred surface densities.

The $N = 1925$ surface densities $\{\sigma_{\text{solid},i}\}$ so computed are displayed against semimajor axes $\{a_i\}$ in Figure 2. The median surface density in each of 20 semimajor axis bins is shown as a red histogram. We fit a power law to the median data — omitting the bin at $a < 0.05$ AU because it contains systems that we consider outliers (see §2.1 regarding our alternate MMEN construction; and also §3.7). This best-fit power law to the median data defines our standard MMEN surface density in solids:

$$\sigma_{\text{solid}} = 6.2 \times 10^2 \mathcal{F}_{\text{disk}} \left(\frac{a}{0.2 \text{ AU}} \right)^{-1.6} \text{ g cm}^{-2}, \quad (4)$$

where $\mathcal{F}_{\text{disk}} \geq 1$ accounts for how much more mass the disk may have relative to the MMEN.

Note that each $\sigma_{\text{solid},i}$ does not depend on such factors as $\mathcal{F}_{\text{transit}}$ or $\mathcal{F}_{\text{detect}}$ (see §1.1). The set of $\{\sigma_{\text{solid},i}\}$ merely represents, by construction, the surface densities of the disks required to form the known planets *in situ*.

Dividing σ_{solid} by $Z_{\text{solar}} \times Z_{\text{rel}}$, where $Z_{\text{solar}} = 0.015$ is the total solar metallicity (Lodders 2003), we find a gas (H and He) surface density of

$$\sigma_{\text{gas}} = 1.3 \times 10^5 \mathcal{F}_{\text{disk}} \left(\frac{a}{0.2 \text{ AU}} \right)^{-1.6} \text{ g cm}^{-2}. \quad (5)$$

In the next two subsections, we consider alternate constructions of the MMEN, using alternate input assumptions.

2.1 Alternative construction of MMEN

A disadvantage to using the median $\{\sigma_{\text{solid},i}\}$ to define the MMEN is that it does not account for relative occurrence rates between semi-major axis bins. In particular, computing the median in each bin does not reflect the fact that planets in the leftmost bin at $a < 0.05$ AU are more rare than those in the neighboring bin (see Figure 2) — an observation which presumably implies real deficits of disk surface density at $a < 0.05$ AU. An alternate construction of the MMEN that does account for such effects is made as follows. We take the $N = 1925$ planets and sort them into semimajor axis bins (assuming, as before, the period-semimajor axis relation for solar-mass stars). Each detected planet is augmented by $N_a = 200 (a/\text{AU})$ additional planets (of the same radius) to account for the geometric probability of transit. Planetary masses are estimated according to the mass-radius relation cited above, and the surface density in each semimajor axis bin is computed by adding together all the mass in that bin and dividing by the annular area corresponding to that bin. The surface density profile is then normalized to a per-star basis by dividing through by the total number of planets summed over all bins (44307 = original plus augmented).

This alternative MMEN is shown as a black histogram in Figure 2. For the most part it tracks our standard MMEN, although it is everywhere lower. At $a \gtrsim 0.05$ AU, we interpret the deficit to reflect incompleteness in the Batalha et al. (2012) catalog — i.e., if $\mathcal{F}_{\text{detect}}$ ranges from 60% at $a \approx 0.2$ AU to 40% at $a \approx 0.4$ AU, then the alternate MMEN would come into alignment with the standard MMEN. At $a \lesssim 0.05$ AU, it seems unlikely that the Batalha et al. (2012) catalog is incomplete (i.e., $\mathcal{F}_{\text{detect}} \approx 1$ at the smallest orbital distances), and the factor of 10 difference between the alternate MMEN and the standard MMEN probably underscores a real paucity of solid material there for most stars. We propose that sublimation of dust is responsible for this deficit (§4.1).

2.2 Sensitivity of the normalization and slope of the MMEN surface density to input assumptions

Taken at face value, the solid surface density σ_{solid} for our MMEN is a factor of 5 larger than the solid surface density of the MMSN — see equation 2 of Chiang & Youdin (2010), and use $Z_{\text{rel}} = 0.33$ for the fraction of metals condensed as solids in the hot inner disk (i.e., metals not taking the form of water; Lodders 2003). As a further point of comparison, our σ_{solid} is a factor of 7 times larger than the surface density in rock as calculated by Hayashi (1981).

These factors by which the MMEN is overdense compared to the MMSN may be mis-estimated as they are sensitive to our assumed mass-radius relation $M = M_\oplus (R/R_\oplus)^{2.06}$. We experiment with two other mass-radius relations. The first is from Wu & Lithwick (2012), who deduced using transit timing variations that close-in super-Earths are better described by $M/M_\oplus \approx 3(R/R_\oplus)^1$ for $R \approx 1\text{--}7R_\oplus$. Using their mass-radius relation, we re-compute the MMEN and find $\sigma_{\text{solid}} = 7.4 \times 10^2 (a/0.2 \text{ AU})^{-1.8} \text{ g cm}^{-2}$, which differs from our equation (4) by about 20%. Looking at Figure 5 of Wu & Lithwick (2012), we see that our fiducial $M \propto R^2$ relation still appears acceptable over the range $R = 2\text{--}5R_\oplus$, which is where we have used it.

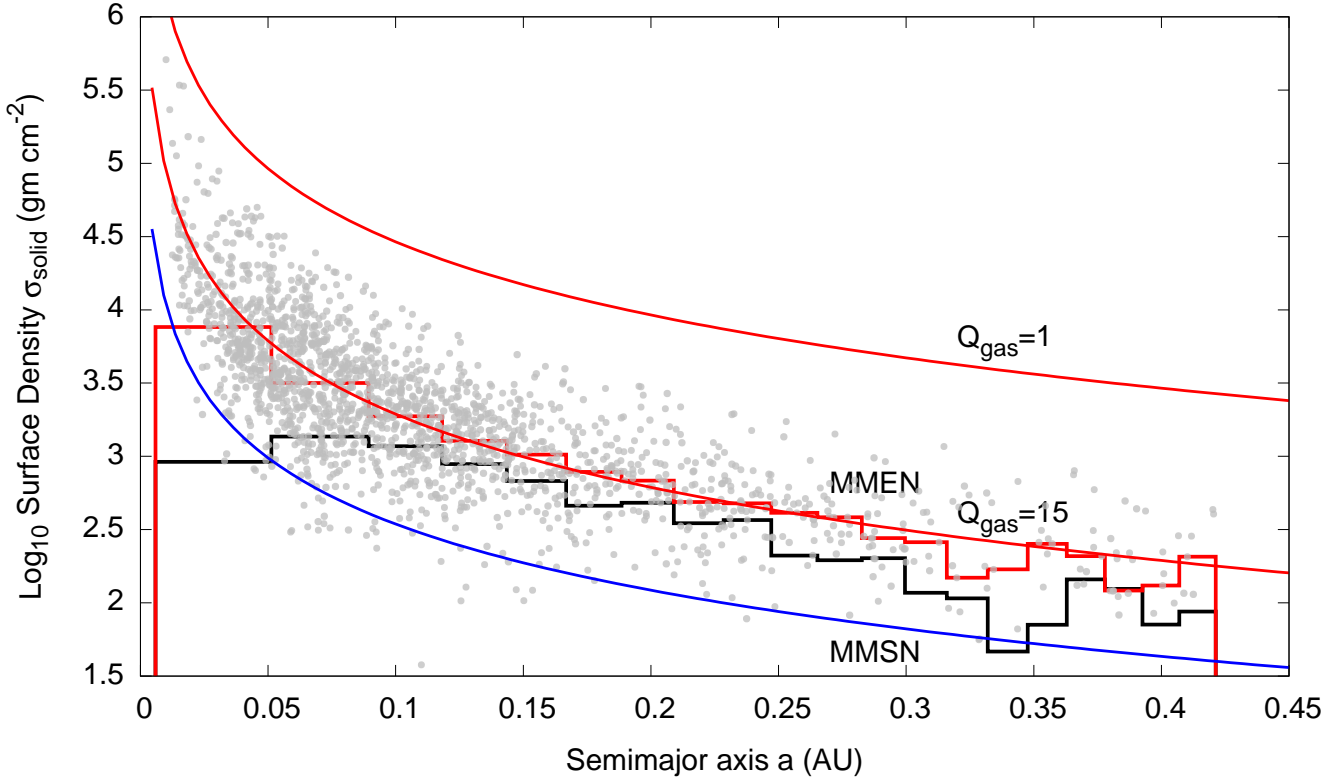


Figure 2. The solid surface density profile of the “minimum-mass extrasolar nebula” (MMEN) constructed from *Kepler* data. *Gray circles:* $\{\sigma_{\text{solid},i}\} \equiv \{M_i/2\pi a_i^2\}$ computed from *Kepler* planets with $R < 5R_{\oplus}$ and $P < 100$ d, assuming $M/M_{\oplus} = (R/R_{\oplus})^{2.06}$ and solar-mass host stars.³ The red histogram is the binned median of the gray points, and the solid red curve is the power law (equation 4) fitted to all red histogram bins except the last bin at $a < 0.05$ AU (see §2.1). The black histogram is an alternate construction of the MMEN (§2.1); we argue that it is lower than the red histogram at $a \gtrsim 0.05$ AU because of incompleteness in the *Kepler* catalog, and also lower at $a \lesssim 0.05$ AU because dust is typically absent at these distances in T Tauri disks and cannot seed planet formation. When enough water (oxygen), H, and He are added to solids to bring the entire MMEN up to solar composition (metallicity = 0.015), the resultant Toomre parameter $Q_{\text{gas}} \approx 15$. If we allow for factors of 2–3 inefficiency in forming planets, then some primordial disks (those populating the upper envelope of gray points) approach the $Q_{\text{gas}} = 1$ threshold for gravitational instability. For reference, σ_{solid} for the minimum-mass Solar nebula (MMSN) — or technically its extrapolation inward, since no planet is present interior to Mercury at $a = 0.4$ AU — is plotted as a blue solid curve. As plotted, the MMEN is a factor of 5 times more massive than the MMSN at these distances, but this factor could be as low as ~ 1 if other mass-radius relations are assumed (§2.2).

Our second experiment uses the mass-radius relations calculated by Rogers et al. (2011) for rocky cores laden with hydrogen envelopes — the kind of planets we expect from an *in-situ* formation scenario (§3.3–§3.4). Combining their Figure 4 with our expressions for envelope-to-core masses as derived in §3.3, and repeating our calculation for the MMEN, we find that $\sigma_{\text{solid}} \approx 1.7 \times 10^2 (a/0.2 \text{ AU})^{-1.6} \text{ g/cm}^2$ — a result that practically coincides with the (extrapolated) MMSN. The surface density drops by a factor of ~ 4 relative to our standard model because the Rogers et al. (2011) planets have extraordinarily low densities (they are “puffy”); for example, a $3R_{\oplus}$ planet with an H-to-rock fraction of 1% might only have a mass of $1.5M_{\oplus}$ according to their Figure 4, because the hydrogen atmosphere is so voluminous.

Another way in which our calculation of σ_{solid} is biased is in the incompleteness of the Batalha et al. (2012) catalog, particularly for small planets. When we incorporate the incompleteness corrections calculated by Dong & Zhu (2012, see their Figure 5) for planets with $1 < R(R_{\oplus}) < 5$, thereby adding many small planets to our analysis, we find that $\sigma_{\text{solid}} = 4.3 \times 10^2 (a/0.2 \text{ AU})^{-1.6} \text{ g/cm}^2$.

We conclude from these experiments that depending on the input assumptions, the factor by which the MMEN is overdense com-

pared to the MMSN may range from ~ 1 to ~ 5 , and that the power-law slope of the disk surface density with orbital radius ranges from -1.6 to -1.8 (compared to the canonical MMSN value of -1.5). From an order-of-magnitude perspective, the MMEN does not appear too different from the MMSN! Our fitted slope can be understood simply in terms of the observations. Since $\sigma_{\text{solid}} \propto M(a)/(a\Delta a)$ and $\Delta a \propto a$, it must be that the characteristic planet mass $M(a) \propto a^{0.3}$ if $\sigma_{\text{solid}} \propto a^{-1.7}$. Indeed such an increase in planet mass with radius is evinced by the data in Figure 1 (and as already noted, the incompleteness corrections of Dong & Zhu 2012 do not much affect this trend).

2.3 Other physical properties of the MMEN

At small stellocentric distances, the energy locally liberated by accretion in a protoplanetary disk raises the midplane temperature significantly above that of a disk passively heated by stellar radiation. If the accretional energy is radiated vertically, the factor by which the midplane temperature is boosted scales as $\tau^{1/4}$, where τ is the Rosseland mean optical depth across the vertical extent of the disk (e.g., Lecar et al. 2006, their equations 1 and 2). Radiative

equilibrium models of actively accreting disks were constructed by, e.g., D’Alessio et al. (1998) and D’Alessio et al. (2001), who found that as the disk radius decreases, the midplane temperature tends to saturate near the dust sublimation temperature of ~ 1500 K; dust vaporizes in hotter disks and throttles the optical depth back down. The radial extent of this near-isothermal zone depends sensitively on the assumed grain size distribution (bigger grains yield smaller optical depths) and on the disk surface density. Note that the surface densities (4)–(5) of our MMEN are about two orders of magnitude larger than those calculated by D’Alessio et al. (2001).

Given the uncertainties, we assume for simplicity an isothermal disk:

$$T = 10^3 \text{ K}. \quad (6)$$

For a disk of this temperature orbiting a solar mass star,⁶ the hydrostatic thickness-to-radius aspect ratio is

$$\frac{h_{\text{gas}}}{a} = \frac{c_{\text{gas}}}{\Omega a} = 0.03 \left(\frac{a}{0.2 \text{ AU}} \right)^{1/2} \quad (7)$$

where c_{gas} is the gas sound speed and Ω is the Kepler orbital frequency. Combining (5) and (7) yields a midplane gas density

$$\rho_{\text{gas}} = \frac{1}{\sqrt{2\pi}} \frac{\sigma_{\text{gas}}}{h_{\text{gas}}} = 6 \times 10^{-7} \mathcal{F}_{\text{disk}} \left(\frac{a}{0.2 \text{ AU}} \right)^{-3.1} \text{ g cm}^{-3}. \quad (8)$$

The Toomre stability parameter (e.g., Binney & Tremaine 2008) for our gas disk is

$$Q_{\text{gas}} = \frac{c_{\text{gas}} \Omega}{\pi G \sigma_{\text{gas}}} = 15 \mathcal{F}_{\text{disk}}^{-1} \left(\frac{a}{0.2 \text{ AU}} \right)^{0.1}, \quad (9)$$

large enough compared to unity that the MMEN is gravitationally stable. Interestingly, if we allow $\mathcal{F}_{\text{disk}} \approx 2\text{--}3$ (i.e., if planet formation were 30–50% efficient), those systems plotted in Figure 2 having the largest surface densities $\{\sigma_{\text{solid},i}\}$ have Toomre parameters Q_{gas} approaching unity (see also §3.7). This suggests that some planets formed in “maximum-mass nebulae” which were on the verge of gravitational instability.

3 ORDERS OF MAGNITUDE

We use the MMEN constructed in §2 to sketch how close-in super-Earths can form *in situ*, working to order-of-magnitude accuracy.

3.1 Close-in super-Earths formed quickly, within gas disk lifetimes

Large disk surface densities σ_{solid} and short dynamical times Ω^{-1} work together to enable close-in rocky planets to coagulate rapidly. Discarding factors of order unity, we estimate that a planetary core of mass M_{core} , radius R_{core} , and bulk density ρ_{core} doubles its mass

⁶ A disk having a gas surface density of $\sigma_{\text{gas}} = 1.3 \times 10^5 \text{ g cm}^{-2}$ (equation 5) at $a = 0.2 \text{ AU}$ could have a midplane temperature of $T = 10^3 \text{ K}$ (equation 6) if the mass accretion rate were $10^{-9} M_{\odot}/\text{yr}$ and the disk opacity were $\sim 0.03 \text{ cm}^2/(\text{g of gas})$. Such a disk opacity safely exceeds the lower bound of $\sim 10^{-3} \text{ cm}^2/\text{g}$ which obtains when grains are completely absent (Freedman et al. 2008).

in a time

$$t_{\text{coagulate}} = \frac{M_{\text{core}}}{\dot{M}_{\text{core}}} \sim \frac{\rho_{\text{core}} R_{\text{core}}^3}{\rho_{\text{solid}} \cdot \mathcal{F}_{\text{grav}} R_{\text{core}}^2 \cdot v_{\text{solid}}} \quad (10)$$

$$\sim \frac{\rho_{\text{core}} R_{\text{core}}}{(\sigma_{\text{solid}}/h_{\text{solid}}) \mathcal{F}_{\text{grav}} v_{\text{solid}}} \quad (11)$$

$$\sim \frac{1}{\mathcal{F}_{\text{grav}}} \frac{\rho_{\text{core}} R_{\text{core}}}{\sigma_{\text{solid}} \Omega} \quad (12)$$

where ρ_{solid} is the mass density of the sea of planetesimals in which the planet is immersed, v_{solid} is the velocity dispersion of planetesimals (assumed to be isotropic and greater than the planet’s epicyclic velocity), $h_{\text{solid}} \sim v_{\text{solid}}/\Omega$ is the vertical thickness of the planetesimal disk, and $\mathcal{F}_{\text{grav}} \geq 1$ is the factor by which gravitational focussing enhances the accretion cross-section above its geometric value (see Goldreich et al. 2004 for a review). For our MMEN parameters, planets form in short order (see also Montgomery & Laughlin 2009 and Hansen & Murray 2012):

$$t_{\text{coagulate}} \sim \frac{2 \times 10^5}{\mathcal{F}_{\text{grav}}} \left(\frac{\rho_{\text{core}}}{6 \text{ g cm}^{-3}} \right) \left(\frac{R_{\text{core}}}{2 R_{\oplus}} \right) \cdot \left(\frac{600 \text{ g cm}^{-2}}{\sigma_{\text{solid}}} \right) \left(\frac{2\pi/\Omega}{30 \text{ days}} \right) \text{ yr} \quad (13)$$

$$\sim \frac{2 \times 10^5}{\mathcal{F}_{\text{grav}}} \left(\frac{R_{\text{core}}}{2 R_{\oplus}} \right) \left(\frac{a}{0.2 \text{ AU}} \right)^{3.1} \text{ yr}. \quad (14)$$

Since $\mathcal{F}_{\text{grav}} \geq 1$, close-in super-Earths can readily form within the lifetimes of inner gas disks, estimated to be $t_{\text{gas}} \sim 10^6\text{--}10^7 \text{ yr}$ from observations of near-infrared excesses of young stellar objects (e.g., Hernández et al. 2008).

We assume throughout this paper that close-in, rocky super-Earths form to completion while the full, solar-abundance complement of gas is still present. This assumption is not without peril. Gas can circularize the orbits of growing protoplanets by dynamical friction, preventing orbits from crossing and halting further mergers. Under these conditions, a protoplanet grows until it is “isolated” — i.e., when it has consumed all the solid material within ~ 2.5 Hill radii of itself (Greenberg et al. 1991). We assume here that dynamical friction cooling by gas does not prevent protoplanets from merging beyond the isolation phase, and that coagulation completes well before the gas disk dissipates — indeed our predictions in §3.3 for the amount of gas accreted by rocky cores will rely on a full gas budget. Our assumption could be justified if the ambient disk is sufficiently turbulent that density fluctuations in gas continuously excite protoplanet eccentricities (see, e.g., section 3.1 of the review by Kley & Nelson 2012), thereby maintaining a chaotic sea of crossing orbits. The eccentricities required for “isolation-mass” embryos to cross orbits are on the order of ~ 0.01 .

3.2 Close-in super-Earths accreted planetesimals each dozens of kilometers in size

The planetesimals accreted by the protoplanets cannot be too small, lest they spiral inward onto the star by aerodynamic drag. The inspiral time, given by the planetesimal’s orbital angular momentum divided by the aerodynamic drag torque, must be longer than $t_{\text{coagulate}}$:

$$t_{\text{inspiral}} \sim \frac{\rho_{\text{bulk}} s^3 \Omega a^2}{\rho_{\text{gas}} v_{\text{rel}}^2 s^2 a} \gtrsim t_{\text{coagulate}} \quad (15)$$

where ρ_{bulk} is the bulk density of a planetesimal, s is the planetesimal size, and v_{rel} is the velocity of gas relative to the planetesimal

(v_{rel} is assumed anti-parallel to the planetesimal's orbital velocity). In writing (15) we have assumed (and have checked *a posteriori*) that the drag force is appropriate for flow around a blunt obstacle at high Reynolds number. To estimate v_{rel} , we recognize that gas is supported by a radial pressure gradient and orbits the star at the sub-Keplerian velocity $(1 - \eta)\Omega a$, where $\eta \sim (h_{\text{gas}}/a)^2 \sim 8 \times 10^{-4} (a/0.2 \text{ AU})^1$ (Adachi et al. 1976; Chiang & Youdin 2010). Taking the planetesimal's orbital velocity to be the full Keplerian value, we find that $v_{\text{rel}} \sim \eta\Omega a \sim 50 \text{ m s}^{-1} (a/0.2 \text{ AU})^{1/2}$. Thus to satisfy (15), the planetesimals must have sizes

$$s \gtrsim \Omega t_{\text{coagulate}} \frac{\rho_{\text{gas}}}{\rho_{\text{bulk}}} \eta^2 a \quad (16)$$

$$\gtrsim 50 \left(\frac{0.2 \text{ AU}}{a} \right)^{1.6} \left(\frac{3 \text{ g cm}^{-3}}{\rho_{\text{bulk}}} \right) \left(\frac{t_{\text{coagulate}}}{2 \times 10^5 / \mathcal{F}_{\text{grav}} \text{ yr}} \right) \text{ km}. \quad (17)$$

How are such super-km-sized planetesimals formed? There is as yet no consensus. Recent work focuses on a combination of aerodynamic and gravitational instabilities to agglomerate particles (Youdin & Goodman 2005; Johansen et al. 2007; Bai & Stone 2010; and references therein) — or on pure gravitational instability of a vertically thin and dense dust layer (Lee et al. 2010a,b; Shi & Chiang 2012).

3.3 Close-in super-Earths accreted hydrogen from the primordial gas disk — typically 3% by mass, up to a maximum of $\sim 1/(2Q_{\text{gas}})$

Immersed in gaseous disks, rocky cores acquire gas envelopes. A protoplanet derives an accretional luminosity from infalling planetesimals, and the gas envelope must transport this energy of accretion. Planetary accretion luminosities are so high (see §3.1), and dust-laden gas in the dense inner disk so optically thick, that the energy is likely transported by convection — i.e., the atmospheres are adiabatic, not isothermal (e.g., Rafikov 2006; Ikoma & Hori 2012). In this case, as long as the gas envelope is not so extended that it becomes truncated by stellar tides (see below), its mass scales with the Bondi radius R_{Bondi} :

$$M_{\text{envelope}} \sim 4\pi\rho_{\text{gas}} R_{\text{Bondi}}^3 \quad (18)$$

where

$$R_{\text{Bondi}} = GM_{\text{core}}/c_{\text{gas}}^2. \quad (19)$$

It follows that

$$\frac{M_{\text{envelope}}}{M_{\text{core}}} \sim \left(\frac{M_{\text{core}}}{M_{\oplus}^*} \right)^2 \sim 3\% \left(\frac{M_{\text{core}}}{4M_{\oplus}} \right)^2 \left(\frac{23M_{\oplus}}{M_{\text{core}}^*} \right)^2 \quad (20)$$

where

$$M_{\text{core}}^* = \frac{c_{\text{gas}}^3}{G^{3/2}(4\pi\rho_{\text{gas}})^{1/2}} = 23 \mathcal{F}_{\text{disk}}^{-1/2} \left(\frac{a}{0.2 \text{ AU}} \right)^{1.55} M_{\oplus}. \quad (21)$$

For fixed M_{core} , the gas-to-rock fraction $M_{\text{envelope}}/M_{\text{core}} \propto \mathcal{F}_{\text{disk}} a^{-3.1}$.

The gas-to-rock fraction implied by equation (20) breaks down for large M_{core} . Cores with

$$M_{\text{core}} \gtrsim M_{\text{Bondi=Hill}} = \frac{c_{\text{gas}}^3 a^{3/2}}{G^{3/2}(3M_{\oplus})^{1/2}} \approx 4 \left(\frac{a}{0.2 \text{ AU}} \right)^{3/2} M_{\oplus} \quad (22)$$

have their gas envelopes truncated by stellar tides: for such massive

cores, R_{Bondi} exceeds

$$R_{\text{Hill}} \sim \left(\frac{M_{\text{core}}}{3M_{\oplus}} \right)^{1/3} a \quad (23)$$

the radius of the Hill sphere surrounding the planet beyond which stellar gravity circumscribes circumplanetary orbits. In this regime, the gas envelope mass attains its maximum value set by R_{Hill} :

$$\max M_{\text{envelope}} \sim 4\pi\rho_{\text{gas}} R_{\text{Hill}}^3 \quad (24)$$

so that

$$\max \frac{M_{\text{envelope}}}{M_{\text{core}}} \sim \frac{4\pi\rho_{\text{gas}} a^3}{3M_{\oplus}} \quad (25)$$

$$\sim 3\% \mathcal{F}_{\text{disk}}^{-1} \left(\frac{a}{0.2 \text{ AU}} \right)^{-0.1} \quad (26)$$

independent of M_{core} . Having the planet's (adiabatically distended) gas envelope truncate at the Hill sphere — which lies well inside the disk scale height h_{gas} for our parameters — reassures that close-in super-Earths do not undergo runaway gas accretion to become gas giants.

Note that equation (25) can be rewritten as

$$\max \frac{M_{\text{envelope}}}{M_{\text{core}}} \sim \frac{4}{3\sqrt{2\pi}} Q_{\text{gas}}^{-1}. \quad (27)$$

Referring back to the curves of constant Q_{gas} overlaid on Figure 2, we see that quite a few super-Earths (those gray points having the highest values of $\sigma_{\text{solid},i}$) could have gas-to-rock fractions of up to $\sim 30\%$.

We caution that the equations in this subsection pertain to adiabatic and not isothermal gas envelopes. Cores at larger disk radii ($a \gg 0.5 \text{ AU}$) typically have lower accretional luminosities (lower planetesimal accretion rates) and are immersed in less optically thick gas. Radiative cooling efficiencies are consequently greater, and render the disk at large a — e.g., at $a = 5 \text{ AU}$ where Jupiter resides — more conducive to runaway gas accretion. See, e.g., Figure 7a of Rafikov (2006).

Clearly, the simple-minded analysis we have presented above for gas-to-rock fractions does not capture a host of effects — gas cooling, spatial and temporal variations in the nebular pressure and temperature beyond those we have assumed, and complicated circumplanetary flows — that could change our answers significantly (see, e.g., Lubow & D'Angelo 2006; Ikoma & Hori 2012). Our intent is merely to show that *in-situ* accretion of gas envelopes is *prima facie* plausible insofar as the order-of-magnitude estimates of gas fractions in equations (20), (25), and (27) are in the same ballpark as those inferred from radius-mass measurements of close-in super-Earths (see, e.g., Figure 6 of Rogers et al. 2011 — but note that these calculated present-day gas fractions are themselves uncertain as they rely on opacities and atmospheric temperature profiles that are not well constrained).

3.4 Many but not all close-in super-Earths retain their primordial hydrogen envelopes

The energy required for a hydrogen atom of mass m_{H} to escape the atmosphere of a super-Earth is $\sim GMm_{\text{H}}/R \sim 2(M/10M_{\oplus})(3R_{\oplus}/R) \text{ eV}$, large enough that only high-energy X-ray and UV (XUV) photons from the parent star can impart the requisite energy by photoionization (by comparison, stellar optical radiation heats particles up to a mean energy $kT_{\text{eff}} \sim 0.06 \text{ eV}$, where

k is Boltzmann’s constant and $T_{\text{eff}} \sim 700$ K is the effective black-body temperature of the planet). We assume that a fraction ϵ of the impinging XUV stellar radiation goes toward lifting gas out of the planet’s gravity well:

$$\epsilon \frac{L_{\text{XUV}}}{4\pi a^2} \cdot \pi R^2 = \frac{GM\dot{M}}{R}. \quad (28)$$

Mass loss in this regime is “energy-limited” (e.g., Murray-Clay et al. 2009). We adopt

$$L_{\text{XUV}} \approx 3 \times 10^{-6} \left(\frac{t}{5 \text{ Gyr}} \right)^{-1.23} L_{\odot} \quad (29)$$

for $t > 0.1$ Gyr (Ribas et al. 2005), and

$$L_{\text{XUV}} \approx 3 \times 10^{-4} L_{\odot} \quad (30)$$

for $t < 0.1$ Gyr. We further take $R = 5R_{\oplus}$ at $t < 0.1$ Gyr to account for how the primordial gas envelope may be distended because of an initially high entropy (cf. Lopez et al. 2012), and set $R = 3R_{\oplus}$ for $t > 0.1$ Gyr. Given these assumptions, most of the mass loss occurs at $t < 0.1$ Gyr, and the amount of mass lost is

$$\Delta M_{\text{envelope}} \sim 0.01 \left(\frac{\epsilon}{0.1} \right) \left(\frac{R}{5R_{\oplus}} \right)^3 \left(\frac{10M_{\oplus}}{M} \right) \left(\frac{0.2 \text{ AU}}{a} \right)^2 M_{\oplus}. \quad (31)$$

This is a factor of 10–100 less than the hydrogen envelope masses imputed to many (but not all) *Kepler* super-Earths based on radius-mass measurements, and it is similarly smaller than the envelope masses we estimated in §3.3. Thus we expect many super-Earths to largely retain their hydrogen envelopes. There is, however, enough variance in the input parameters that we would also expect some planets (having some combination of small a , small M_{envelope} , or large incident XUV flux) to be stripped clean of their hydrogen veneers.⁷ Individual cases are discussed in §3.7.

3.5 Close-in super-Earths stay in place after formation

Super-Earths formed at small stellocentric distances have not much choice but to stay there. They cannot scatter each other out of the gravity well of the star, because the largest velocity dispersion they can attain by mutual scatterings is set by their mutual surface escape velocity

$$v_{\text{esc}} \sim 20 \left(\frac{M_1 + M_2}{20M_{\oplus}} \right)^{1/2} \left(\frac{6R_{\oplus}}{R_1 + R_2} \right)^{1/2} \text{ km s}^{-1} \quad (32)$$

which is less than the escape velocity from the star

$$v_{\text{esc},*} \sim 90 \left(\frac{0.2 \text{ AU}}{a} \right)^{1/2} \text{ km s}^{-1}. \quad (33)$$

Thus dynamical instabilities — i.e., planet-planet scatterings — in the inner disk do not result in ejection but rather in planet-planet mergers (or, in rare instances, tidal interactions with the star and orbital decay).

In-situ formation predicts that an “oligarchy” composed of closely nested protoplanets eventually destabilizes when the oligarchs viscously stir themselves faster than the underlying disk can cool them by dynamical friction (e.g., Kokubo & Ida 2000; Goldreich et al. 2004; Kenyon & Bromley 2006; Ford & Chiang 2007).

Oligarchs ultimately scatter each other onto crossing orbits. The inequality $v_{\text{esc}} < v_{\text{esc},*}$ implies that in the ensuing chaos, protoplanets coalesce — with the mass-doubling time t_{coag} given by the relations in §3.1. The total number of bodies decreases and the rate of scattering declines. The final set of super-Earths will occupy, at first, orbits with eccentricities and inclinations up to $v_{\text{esc}}/v_{\text{esc},*} \sim 0.2$; these will be circularized and flattened by any residual disk of planetesimals (§3.6). The leftover disk of solids will, in turn, eventually be consumed by the planets, at least in part.

Since ambient gas does not accrete in runaway fashion onto protoplanet cores (§3.3), and since photoevaporation is not efficient at removing gas at small orbital radii (gas cannot be heated to the temperatures of $\sim 10^6$ K required for c_{gas} to approach $v_{\text{esc},*}$), gas that is not bound to cores in the inner disk has no option but to accrete onto the star. The mechanism of disk accretion is uncertain, but the magnetorotational instability is arguably viable in these hot and relatively well-ionized regions (cf. Bai 2011 and Perez-Becker & Chiang 2011a,b for difficulties with appealing to the magnetorotational instability for the rest of the disk).

3.6 Close-in super-Earths currently reside in co-planar and nearly circular orbits

Once disk gas dissipates to the point where its turbulent density fluctuations no longer perturb super-Earths significantly (§3.1), the remaining planets have their orbital inclinations and eccentricities damped by dynamical friction with leftover planetesimals. The velocity dispersion of residual planetesimals is, in turn, damped by inelastic collisions and/or drag by remaining gas. The leftover disk of solids need only be a small fraction of the original disk of solids to circularize and flatten planetary orbits. An initial planetary eccentricity e_{init} damps to zero over a time

$$t_{\text{circularize}} \sim 0.1 \frac{M_*}{M} \frac{\Omega a}{G\sigma_{\text{leftover}}} e_{\text{init}}^4 \quad (34)$$

$$\sim 2 \times 10^5 \left(\frac{10M_{\oplus}}{M} \right) \left(\frac{6 \text{ g cm}^{-2}}{\sigma_{\text{leftover}}} \right) \cdot \left(\frac{a}{0.2 \text{ AU}} \right) \left(\frac{e_{\text{init}}}{0.1} \right)^4 \text{ yr} \quad (35)$$

(e.g., Ford & Chiang 2007; the pre-factor of 0.1 contains a Coulomb-type logarithm). An analogous formula applies for damping the mutual inclination between the planetary orbit and the disk of planetesimals.

Because eccentricities and inclinations are so readily damped by leftover planetesimals, we expect close-in super-Earths to occupy nearly circular, coplanar orbits. A hard lower bound on the final eccentricities will be established by gravitational interactions between the planets *in vacuo*. A lower bound on the mutual inclinations is less clear, as a system that is perfectly coplanar will remain so forever. The final eccentricities and inclinations will depend not only on how strongly planets stir one another during the post-oligarchic phase of planet formation — and the stirring rate is a sensitive function of oligarchic mass and spacing (Chambers et al. 1996; Ford & Chiang 2007) — but also on the rate at which the leftover disk dissipates. At least in the case of the Solar System’s giant planet satellites, eccentricities are typically of the same order of magnitude as inclinations.

⁷ Giant impacts may also erode atmospheres; see §3.5.

3.7 Some extreme extrasolar systems

We consider now some specific examples of super-Earths that have garnered special attention in recent years. We apply the order-of-magnitude analyses in previous subsections to assess the possibility that these planets formed *in situ*. Some properties of these planets will be found to lie at the extremities of parameter space, and we will identify arguments both for and against *in-situ* accretion.

3.7.1 The Kepler-11 system (b–f)

The innermost five planets of the Kepler-11 system have a total mass of $M_{\text{tot}} \approx 35M_{\oplus}$ between $a_1 = 0.09$ AU and $a_2 = 0.25$ AU around a solar-mass star (Lissauer et al. 2011a). If we assume that the planets are composed predominantly of rock (see Figure 5 of Lissauer et al. 2011a), then the solid surface density of the “minimum-mass Kepler-11” system is $\sigma_{\text{solid}} \sim M_{\text{tot}}/2\pi a_2^2 \sim 2.4 \times 10^3 \text{ g cm}^{-2}$, about 6 times larger than that of the MMEN at $a = 0.25$ AU. For a solar metallicity disk, the Toomre parameter $Q_{\text{gas}} \sim 2.5$, suggesting that the Kepler-11 primordial disk may have been on the verge of gravitational instability — i.e., it may have been a “maximum-mass” nebula. The packed set of planets is reminiscent of an oligarchy (e.g., Kokubo & Ida 2000; Goldreich et al. 2004).

Substituting the parameters of the Kepler-11 disk into equations (20)–(27), we expect the primordial H-He mass fraction of a Kepler-11 planet to range from

$$\frac{M_{\text{envelope}}}{M_{\text{core}}} \sim 4\% \left(\frac{M_{\text{core}}}{2M_{\oplus}} \right)^2 \left(\frac{a}{0.2 \text{ AU}} \right)^{-3.1} \quad (36)$$

for $M_{\text{core}} < M_{\text{Bondi=Hill}} \approx 4(a/0.2 \text{ AU})^{3/2} M_{\oplus}$ (this is the case for planet f), to a maximum gas fraction of

$$\max \frac{M_{\text{envelope}}}{M_{\text{core}}} \sim 20\% \left(\frac{2.5}{Q_{\text{gas}}} \right) \quad (37)$$

for $M_{\text{core}} > M_{\text{Bondi=Hill}}$ (planets b, c, d, and e). Our estimates of primordial gas-to-rock fractions are consistent to order-of-magnitude with interior models that assume gas envelopes overlying rocky cores: to wit, the interior models for Kepler-11c, d, e, and f are characterized by gas-to-rock fractions of 2–20% (Lopez et al. 2012).

An outlier is Kepler-11b, which has the smallest inferred H fraction of $M_{\text{envelope}}/M_{\text{core}} \sim 0.05$ –1.4% (Lopez et al. 2012). At least in principle, this small amount of H may be what remains of a once-massive atmosphere whittled down by XUV photoevaporation. From equation (37) we expect that Kepler-11b could have once had an atmosphere amounting to $\sim 20\%$ of the total planet mass, while equation (31) predicts that XUV radiation could have eroded away $\Delta M_{\text{envelope}} > 0.1M_{\oplus}$ or $> 2\%$ of the planet mass — this is a lower limit because Kepler-11b could have undergone “run-away” mass loss during which the planet stayed inflated for long duration (Baraffe et al. 2004). In fact, Lopez et al. (2012) surmised that if Kepler-11b formed strictly *in situ* and is not a water world, then it started with an enormous initial gas fraction of $\sim 90\%$ in order to retain its currently thin veneer of hydrogen; these authors actually argued against *in-situ* formation because such a large initial planet mass would have threatened the orbital stability of the system. More work is required before the case of Kepler-11b is resolved; the large parameter space of atmospheric opacities, cooling

histories, and planetary magnetic fields (Adams 2011) would seem to allow a wide range of mass loss histories.⁸

3.7.2 Kepler-10b

Kepler-10b is a rocky super-Earth of mass $M = 4.56M_{\oplus}$, $R = 1.42R_{\oplus}$, and bulk density $\rho = 8.8^{+2.1}_{-2.9} \text{ g cm}^{-3}$, orbiting a solar-mass star with a period of 0.836 days and a semimajor axis $a = 0.0168$ AU (Batalha et al. 2011). Our estimate of the surface density of the “minimum-mass Kepler-10b” disk is $\sigma_{\text{solid}} \sim M/2\pi a^2 = 7 \times 10^4 \text{ g cm}^{-2}$. This is 2–3 orders of magnitude larger than the surface density of the MMEN in the smallest semimajor axis bin ($a < 0.05$ AU; Figure 2) and is a measure of just how unusual Kepler-10b is. Nevertheless, the Toomre parameter for the corresponding solar metallicity disk is $Q_{\text{gas}} \sim 6$, large enough for the primordial gas disk to remain gravitationally stable.

Kepler-10b’s large bulk density — between that of compressed iron and a bulk Earth-like composition (Batalha et al. 2011) — indicates that it does not have as much C and O as would be expected for a planet that congealed outside the methane/water ice-lines in the primordial disk. Thus the inferred bulk composition of Kepler-10b argues against wholesale orbital migration.

The mass-doubling time for Kepler-10b is astonishingly short (see equation 13):

$$t_{\text{coagulate}} \sim 30 (R/1.4R_{\oplus}) \mathcal{F}_{\text{grav}}^{-1} \text{ yr}. \quad (38)$$

Most of the time building Kepler-10b was probably spent forming the seed planetesimals (via an unknown mechanism; §3.2). Indeed $t_{\text{coagulate}}$ is so short compared to the typical lifetimes of gas disks ($t_{\text{gas}} \sim 10^6 \text{ yr}$) that the planet almost certainly did not assemble early in the gas disk’s evolution; so much angular momentum and mass must have been transported across the inner disk that it is hard to imagine how early-formed planets could have avoided being torqued by the disk. An *in-situ* accretion scenario for fast-growing objects like Kepler-10b appears to demand that they form at the very end of the gas disk’s life.

Kepler-10b is situated so close to its parent star that stellar XUV radiation likely removed any hydrogen atmosphere it accreted from the parent disk. Plugging the parameters of Kepler-10b into equation (31), we see that enough XUV radiation was deposited to remove up to $\Delta M_{\text{envelope}} \sim 2M_{\oplus}$ or $\sim 40\%$ of its total mass. Kepler-10b probably never had this much hydrogen. The planet’s mass exceeds $M_{\text{Bondi=Hill}} = 0.1(a/0.017 \text{ AU})^{3/2} M_{\oplus}$ (equation 22), and therefore its primordial gas fraction was at most $\sim 9\%$ ($6/Q_{\text{gas}}$) (equation 27). Thus it is not surprising that Kepler-10b can be modeled today as a pure rock planet.

3.7.3 GJ 1214b

GJ 1214b is a super-Earth of mass $M = 6.55M_{\oplus}$, $R = 2.68R_{\oplus}$, and bulk density $\rho = 1.87 \pm 0.4 \text{ g cm}^{-3}$, orbiting an M dwarf of mass

⁸ The possibility that Kepler-11b’s present-day atmosphere results from ongoing outgassing is not viable, because outgassing requires chemical reactions between surface iron and water, neither of which is available. Water is not available because water should not condense in the hot inner nebula, and iron is not available at the planet surface because it is rapidly sequestered in the planetary core soon after the planet’s formation. These same remarks apply for GJ 1214b (§3.7.3).

$M_* = 0.157M_\odot$ and luminosity $L_* = 3 \times 10^{-3}L_\odot$ with a period of 1.58 days and a semimajor axis $a = 0.014$ AU (Charbonneau et al. 2009). An estimate of the surface density of the “minimum-mass GJ 1214b” disk is $\sigma_{\text{solid}} \sim M/2\pi a^2 = 1.4 \times 10^5 \text{ g cm}^{-2}$. This surface density is not readily compared against the MMEN because the MMEN is constructed as an average over solar-mass stars, not M dwarfs like GJ 1214. The Toomre parameter for the corresponding solar metallicity disk is $Q_{\text{gas}} \sim 1.4$ — possibly signaling a system that spent some time on the brink of gravitational instability.

Differences in the mean molecular weight of an atmosphere lead to differences in atmospheric scale height, and these can be distinguished by measuring transit depths as a function of wavelength (Miller-Ricci et al. 2009). Such measurements have been made of GJ 1214b, from wavelengths $\lambda = 0.6 \mu\text{m}$ to $5 \mu\text{m}$ (Bean et al. 2010; Désert et al. 2011; Croll et al. 2011; Bean et al. 2011; Berta et al. 2012; de Mooij et al. 2012). Most of these observations indicate no significant variation of transit depth with wavelength, which *prima facie* points to a massive and high molecular weight atmosphere (made, e.g., of CO_2 ; Lloyd & Pierrehumbert 2013, submitted). This is seemingly incompatible with strict *in-situ* accretion. But in a less strict *in-situ* scenario, sizable ice-rich planetesimals could have migrated inward from outside the carbon/oxygen condensation radii in the primordial disk and assembled into close-in planets at their current orbital distances (Hansen & Murray 2012). Planetesimals that are large enough (i.e., much larger than dust grains) would have sublimation times exceeding coagulation times and would thus be safe against vaporization.

Yet another interpretation is that the atmosphere actually does have a significant H component, but that its flat transmission spectrum arises from hazes (made possibly of KCl or ZnS; Morley et al., in preparation). More data are forthcoming for GJ 1214b (there is, e.g., a 60-orbit *Hubble Space Telescope* campaign led by J. Bean), and whether some form of *in-situ* accretion can be reconciled with the data remains to be seen.

4 PROSPECTS AND PREDICTIONS

Over the past two decades, extrasolar planets have completed their migration from the fringe to the mainstream of astronomy. Time and again, they have defied theoretical predictions regarding their properties in nearly every corner of parameter space. It may be that the community’s state of near-continual surprise stems from an ingrained appeal to our Solar System as our standard template. In this heliocentric view, the default position is to regard extrasolar systems as exotica. We have shown, however, that the close-in super-Earths detected in abundance by the *Kepler* mission and Doppler velocity surveys cannot be viewed this way: more than half, if not nearly all Sun-like stars in the Galaxy harbor planets with radii $2R_\oplus < R < 5R_\oplus$ and periods $P < 100$ d. Super-Earths are not anomalous; they are the rule that our Solar System breaks. In a sense, the burden of explaining planetary system architectures rests more heavily on the Solar System than on the rest of the Galaxy’s planet population at large.

The omnipresent close-in super-Earths enable us to construct a new template, the minimum-mass extrasolar nebula (MMEN), which in turn can be used to explore the possibility that such planets formed *in situ*. Our order-of-magnitude sketches in this regard are promising. *In-situ* formation at small stellocentric distances has all the advantages that *in-situ* formation at large stellocentric distances

does not: large surface densities, short dynamical times, and the deep gravity well of a parent star that keeps its planetary progeny in place.⁹ The large surface densities of the MMEN, if extrapolated to greater stellocentric distances, would also help to form distant gas and ice giants — for a theoretical perspective, see the disk-mass enhancement factors invoked to form Jupiter (e.g., Lissauer et al. 2009) and Uranus and Neptune (e.g., Goldreich et al. 2004), and for an observational view, see the microlensing surveys which report order-unity occurrence rates for super-Earths and gas giants from 0.5–10 AU (Gaudi 2012, his section 6.2). The biggest challenge for theories of planet formation — and this is true regardless of whether planets migrated or not — is in understanding how seed planetesimals form, i.e., how objects grow from sub-cm sizes to super-km scales.

Our unfinished theories of planetesimal formation notwithstanding, the basic properties of close-in super-Earths that form at their current orbital distances seem clear. *In-situ* formation with no large-scale migration generates short-period planets with a lot of rock and metal and very little water. The accretion of nebular gas onto protoplanetary cores of metal produces H/He-rich atmospheres of possibly subsolar metallicity that expand planets to their observed radii. Retainment of primordial gas envelopes against photoevaporation leads to planets that can be similar in bulk density to Uranus and Neptune while being markedly different in composition. Close-in planets are not water worlds (but see the discussion under §3.7.3 for a way to produce close-in water worlds in a less strict *in-situ* formation scenario).

We are all too aware that predictions in the subject of planet formation have a poor track record. Nevertheless, in the firm conviction that good theories are falsifiable ones, we offer here a set of observationally testable consequences of *in-situ* formation, with the aim of bringing the ongoing debate about planetary origins into sharper focus. As we will see, the prospects for further probing many of our ideas are bright.

4.1 Early type stars should lack close-in rocky super-Earths

The *in-situ* formation hypothesis depends on the availability of dust to form seed planetesimals. Where it is too hot for dust to survive, there should be no planets.

How does the “dust-line” (i.e., the radius inside of which dust is vaporized) vary with stellar mass? Near-infrared interferometric measurements indicate that dust-lines expand with increasing stellar luminosity, from 0.05–0.1 AU in the case of T Tauri stars, to 0.1–0.5 AU for Herbig Ae stars, to 0.5–10 AU for Herbig Be stars (see Figure 7 of the review by Dullemond & Monnier 2010). Under *in-situ* formation, the prediction is clear: hotter stars should have fewer planets closer in.

Dust sublimation offers a simple explanation of the dramatic drop in the occurrence rate of super-Earths at $a < 0.05$ AU (§2.1). The drop at $a < 0.05$ AU applies to Sun-like stars, whose progenitors are closest to the T Tauri population.

Our prediction that main-sequence A and B stars — the descendants of Herbig Ae and Be stars — host fewer close-in super-Earths finds some preliminary support in the *Kepler* data. Among

⁹ Another way to say this is that “particle-in-a-box” simulations of planetary coagulation are adequate in the innermost regions of protoplanetary disks, as material is confined to the “box” of the star’s potential well.

stars in the *Kepler* Input Catalog for which (1) photometric light curve data exist, (2) estimates of stellar effective temperature T_{eff} are tabulated, and which are (3) not flagged as red giants, we find that only 2 out of 1965 stars with $7500 \text{ K} < T_{\text{eff}} < 10000 \text{ K}$ harbor planetary candidates with $2.5 R_{\oplus} < R < 5 R_{\oplus}$. On the other hand, among 131,987 primaries with $T_{\text{eff}} < 6000 \text{ K}$, there are 549 candidate planets with $2.5 R_{\oplus} < R < 5 R_{\oplus}$ — a rate that is more than four times higher than the planetary occurrence rate for presumably early-type stars. While this comparison is crude and ignores a host of selection and other potential biases, it is nevertheless consistent with our expectation, and motivates an improved analysis.

4.2 Brown dwarfs and M dwarfs should be accompanied by close-in super-Earths and Earths

If the resemblance noted in §1.2 between close-in super-Earths and giant planet satellites is not a coincidence, then simple interpolation leads to the expectation that stars at the bottom of the main sequence, and brown dwarfs, will be commonly accompanied by planets (satellites) with masses $M \sim 10^{-5} - 10^{-4} M_*$ and $P \lesssim 100$ days. Such low-luminosity primaries are outstanding hosts for *in-situ* planet formation for the same reason that massive early-type stars are not — dust can only survive, and by extension planets can only exist, where disks are cool enough.

For a red dwarf primary of mass $M_* \sim 0.1 M_{\odot}$ and $R_* \sim 0.1 R_{\odot}$, we might expect planet masses $M \sim 10^{-5} - 10^{-4} M_*$ and radii $R \sim 0.7 - 1.5 R_{\oplus}$. The corresponding transit depths are encouragingly large, $(R/R_*)^2 \sim 0.004 - 0.02$. The MEarth Project (Nutzman & Charbonneau 2008) is an ongoing transit survey of up to ~ 2000 M dwarfs. The geometric probability of transit for a $P = 10$ d companion orbiting a $0.1 M_{\odot}$ primary is $\mathcal{F}_{\text{transit}} \sim 1\%$, suggesting that up to a few dozen transiting systems might eventually be detected. The MEarth Project currently sets exposure times to detect planets with $R = 2 R_{\oplus}$ at 3σ confidence (Berta et al. 2012). If the naive and simple-minded scalings we have discussed above hold, then exposure times would need to be adjusted upward to gain access to the bulk of the planets arising from *in-situ* formation and having $R < 2 R_{\oplus}$.

4.3 Stellar binaries can be used to rule out migration

Planets cannot form at large distance from a star if that star is orbited by a close enough companion. Gravitational perturbations from a stellar companion can destabilize certain swaths of circumstellar space. In destabilized regions, planetesimals can be excited to such large velocity dispersions that they erode upon colliding. For example, in the protoplanetary disk of Alpha Centauri B, perturbations from star A on its $P = 80$ yr, $e = 0.5$ orbit can thwart planet formation by grinding planetesimals to dust at disk radii $a \gtrsim 0.5$ AU (Th  bault et al. 2009, cf. Rafikov 2012 who notes that the boundary for erosive collisions depends also on disk self-gravity). Were planets ever to be discovered orbiting Alpha Cen B just inside the $a \approx 0.5$ AU boundary, they would be incompatible with long-distance inward migration. The prospects for using stellar binaries to distinguish between *in-situ* formation and migration appear encouraging; Dumusque et al. (2012) have just announced the discovery of a $1.1 M_{\oplus}$ planet in an orbit with semimajor axis $a \approx 0.04$ AU about Alpha Cen B.

Objects at the bottom of the main sequence that are members of wide stellar binaries can undergo *one-time* eclipses during the

course of large-scale photometric surveys. Should the orbital geometry cooperate, a low-mass star can haul its retinue of satellites across the face of a more luminous star. The slow pace of the eclipse (e.g., a central transit of a $1 M_{\odot}$ primary by a companion with $a = 5$ AU lasts 30 hours) improves detection signal-to-noise for satellites of the low-mass secondary. A back-of-the-envelope estimate for the number of one-time eclipses of G dwarfs by low-mass (M dwarf or brown dwarf) companions that *Kepler* might observe is

$$N_{\text{one-time}} \approx 9 \left(\frac{\mathcal{F}_{\text{binary}}}{0.6} \right) \left(\frac{\mathcal{F}_{\text{period}}}{0.1} \right) \left(\frac{\mathcal{F}_{\text{transit}}}{10^{-3}} \right) \left(\frac{N_{*,\text{total}}}{1.56 \times 10^5} \right), \quad (39)$$

where $\mathcal{F}_{\text{binary}}$ is the fraction of G dwarfs with low-mass companions; $\mathcal{F}_{\text{period}}$ is the fraction of such binaries with orbital periods between ~ 3 and 30 yr; and $\mathcal{F}_{\text{transit}}$ is the transit probability normalized to a binary separation of $5 \text{ AU} \sim 10^3 R_*$ (Duquennoy & Mayor 1991). During each of these one-time eclipse events, transits of the G dwarf by planets orbiting the low-mass dwarf are guaranteed if the planets' orbital planes are nearly aligned with the stellar binary orbital plane. Even if a given planetary plane is randomly oriented with respect to the stellar binary plane, the probability of catching a planetary transit drops only by a factor of $\sim \pi/9$. For the proposed *Transiting Exoplanet Survey Satellite* (TESS) Mission (Ricker et al. 2010), which will survey $N_{*,\text{total}} \sim 2 \times 10^6$ stars, $N_{\text{one-time}} \sim 10^2$.

4.4 Orbit normals of close-in super-Earths should be aligned with stellar spin axes

Basic considerations of angular momentum dictate that close-in protoplanetary disks, and the close-in planets that they breed, should have orbital planes that are well-aligned with the equatorial planes of their host stars.¹⁰ This is an eminently testable prediction for *Kepler* planet-bearing systems. Although Rossiter-McLaughlin measurements are too difficult to make for most super-Earths, the stellar equatorial inclinations i_* relative to the sky plane can be determined by conventional means (Hirano et al. 2012). A single high-resolution, high signal-to-noise spectrum can be used to obtain a given star's projected rotational velocity $v_{\text{rot}} \sin i_*$ and radius R_* . In addition, the *Kepler* light curve yields the stellar rotation period P_{rot} . With such measurements in hand,

$$i_* = \arcsin \left(\frac{P_{\text{rot}} \cdot v_{\text{rot}} \sin i_*}{2\pi R_*} \right). \quad (40)$$

In-situ formation predicts that transiting planets should orbit stars for which $i_* \sim 90^\circ$. Because only one spectrum is required per star, this test can be carried out for a large number of targets.

4.5 Close-in super-Earths have primordial H/He atmospheres

Close-in “water worlds” — planets with substantial components of O, C, and N-rich ices, like Neptune¹¹ — are ruled out under strict

¹⁰ Of course, smooth disk-driven migration can also produce spin-aligned orbits. But smooth convergent migration is also expected to produce a preponderance of planets locked in mean-motion resonances, and this is not observed (for a variety of perspectives on this issue, see Lithwick & Wu 2012; Batygin & Morbidelli 2012; Rein 2012; Petrovich et al. 2012).

¹¹ Many papers distinguish between “water worlds” with water-rich surface layers and “hot Neptunes” with hydrogen-rich atmospheres. Throughout our paper we do not follow this practice because Neptune actually con-

in-situ formation because such ices could not have condensed in the hot inner regions of protoplanetary disks (but see §3.7.3 for a less strict scenario). We have shown that close-in super-Earths embedded in their parent gas disks can accrete H/He-rich gas envelopes weighing from a few percent to tens of percent of the planet mass (§3.3). We have also argued that many but not all such planets retain their atmospheres against photoevaporation (§3.4). These expectations are currently in tension with Kepler-11b (§3.7.1) and GJ 1214b (§3.7.3). Spectroscopic measurements of GJ 1214b, HD 97658b, and 55 Cnc e are forthcoming with the *Hubble Space Telescope* (Cycle 20, PI: J. Bean). More super-Earths should also be discovered transiting bright primaries and be amenable to spectroscopic follow-up. For example, Bonfils et al. (2012) have recently announced the detection of GJ 3470b, a planet with $M = 14M_{\oplus}$ and $R = 4.2R_{\oplus}$ orbiting a spectral type M1.5 V host.

4.6 Super-Earths that retain primordial gas atmospheres should be centrally concentrated with small $k_2 \lesssim 0.05$

A rocky planet with an extended H atmosphere is more centrally condensed than a water world with a volatile-rich mantle or atmosphere. Higher degrees of central condensation map to smaller values of the tidal Love number, k_2 . To get a sense of what k_2 -values we may expect for close-in super-Earths, we look to the interior models by Kramm et al. (2011) of GJ 436b ($M \approx 22M_{\oplus}$, $R \approx 4.3M_{\oplus}$, $a \approx 0.03$ AU). For pure H atmospheres overlying massive cores with $M_{\text{core}}/M > 80\%$ — these H-atop-rock solutions are the ones favored by our *in-situ* formation scenario — Kramm et al. (2011) calculated that $k_2 < 0.05$. By contrast, for Neptune (which consists of an H atmosphere draped over a thick water layer, which in turn overlays a rocky core for which $M_{\text{core}}/M < 0.25$), $k_2 \approx 0.16$. Our expectation that $k_2 \lesssim 0.05$ applies only to those close-in super-Earths that retain the sizable H envelopes (§3.3) accreted from the primordial gas disk. Those few pure-rock close-in super-Earths whose atmospheres were obliterated by photoevaporation have relatively homogeneous interiors and thus larger k_2 (e.g., for the Earth, $k_2 \approx 0.3$).

In a tidally evolved, two-planet system, it is possible to infer k_2 for the inner planet (Batygin et al. 2009). Tidal dissipation drives such a system to a fixed point for which the eccentricities cease to exhibit secular oscillations and the apsidal lines of the two planets precess at the same rate (Wu & Goldreich 2002; Mardling 2007). The apsidal precession rate of the inner planet depends on a number of effects: general relativity; secular forcing by the outer planet; the rotational bulge of the inner planet (assumed to be in synchronous rotation with its orbit); and finally the tidally distorted figure of the inner planet. The latter two effects depend on k_2 . By careful measurement of the Keplerian orbital elements via high-quality transit and Doppler observations, the total precession rate can be directly evaluated, as can all of the individual contributions to the inner planet's precession rate — all except those contributions that depend on k_2 , whose value can then be backed out.

To date this method has been applied to the HAT-P-13 b-c system, revealing that the inner hot Jupiter has $0.265 < k_2 < 0.379$ and

$M_{\text{core}} < 27M_{\oplus}$ (Batygin et al. 2009; Kramm et al. 2012). Extension of the method to close-in super-Earths should be possible, particularly with TESS (Ricker et al. 2010).

ACKNOWLEDGMENTS

We thank Jacob Bean, Peter Bodenheimer, Josh Eisner, Jonathan Fortney, Uma Gorti, Richard Greenberg, Edwin Kite, Marc Kuchner, Eric Lopez, Geoff Marcy, Chris Ormel, Margaret Pan, Ilaria Pascucci, Erik Petigura, Sean Raymond, Damien Ségransan, Angie Wolfgang, and Andrew Youdin for helpful discussions. An anonymous referee provided a detailed report that led to substantive changes in this paper. EC acknowledges support from NSF grant AST-0909210. GL acknowledges support from NASA grant NNX11A145A. This study was fostered by the Bay Area Consortium for Exoplanet Science (BACES), whose members include NASA Ames, Berkeley, UC Santa Cruz, and the SETI Institute.

REFERENCES

- Adachi, I., Hayashi, C., & Nakazawa, K. 1976, *Progress of Theoretical Physics*, 56, 1756
- Adams, F. C. 2011, *ApJ*, 730, 27
- Alibert, Y., Baraffe, I., Benz, W., et al. 2006, *A&A*, 455, L25
- Bai, X.-N. 2011, *ApJ*, 739, 50
- Bai, X.-N. & Stone, J. M. 2010, *ApJ*, 722, 1437
- Baraffe, I., Selsis, F., Chabrier, G., et al. 2004, *A&A*, 419, L13
- Batalha, N. M., Borucki, W. J., Bryson, S. T., et al. 2011, *ApJ*, 729, 27
- Batalha, N. M., Rowe, J. F., Bryson, S. T., et al. 2012, *ArXiv e-prints*
- Batygin, K., Bodenheimer, P., & Laughlin, G. 2009, *ApJ Letters*, 704, L49
- Batygin, K. & Morbidelli, A. 2012, *ArXiv e-prints*
- Bean, J. L., Désert, J.-M., Kabath, P., et al. 2011, *ApJ*, 743, 92
- Bean, J. L., Miller-Ricci Kempton, E., & Homeier, D. 2010, *Nature*, 468, 669
- Berta, Z. K., Charbonneau, D., Désert, J.-M., et al. 2012, *ApJ*, 747, 35
- Binney, J. & Tremaine, S. 2008, *Galactic Dynamics: Second Edition*, 2nd edn. (Princeton University Press)
- Bonfils, X., Gillon, M., Udry, S., et al. 2012, *A&A*, 546, A27
- Chambers, J. E., Wetherill, G. W., & Boss, A. P. 1996, *Icarus*, 119, 261
- Charbonneau, D., Berta, Z. K., Irwin, J., et al. 2009, *Nature*, 462, 891
- Chiang, E. & Youdin, A. 2010, *Annual Reviews of Earth and Planetary Science*, 38
- Croll, B., Albert, L., Jayawardhana, R., et al. 2011, *ApJ*, 736, 78
- D'Alessio, P., Calvet, N., & Hartmann, L. 2001, *ApJ*, 553, 321
- D'Alessio, P., Canto, J., Calvet, N., & Lizano, S. 1998, *ApJ*, 500, 411
- de Mooij, E. J. W., Brogi, M., de Kok, R. J., et al. 2012, *A&A*, 538, A46
- Désert, J.-M., Bean, J., Miller-Ricci Kempton, E., et al. 2011, *ApJ Letters*, 731, L40
- Dong, S. & Zhu, Z. 2012, *ArXiv e-prints*
- Dullemond, C. P. & Monnier, J. D. 2010, *ARA&A*, 48, 205
- Dumusque, X., Pepe, F., & Lovis, C., Ségransan, D., et al. 2012, *Nature*, 11572, 1
- Duquennoy, A. & Mayor, M. 1991, *A&A*, 248, 485
- Fabrycky, D. C., Lissauer, J. J., Ragozzine, D., et al. 2012, *ArXiv e-prints*
- Fang, J. & Margot, J.-L. 2012, *ArXiv e-prints*
- Fernandez, J. A. & Ip, W.-H. 1984, *Icarus*, 58, 109
- Figueira, P., Marmier, M., Boué, G., et al. 2012, *A&A*, 541, A139
- Ford, E. B. & Chiang, E. I. 2007, *ApJ*, 661, 602
- Freedman, R. S., Marley, M. S., & Ladders, K. 2008, *ApJ Supplement Series*, 174, 504
- Gaudi, B. S. 2012, *ARA&A*, 50, 411
- Goldreich, P., Lithwick, Y., & Sari, R. 2004, *ARA&A*, 42, 549
- Goldreich, P., Murray, N., Longaretti, P. Y., & Banfield, D. 1989, *Science*, 245, 500

- Greenberg, R., Bottke, W. F., Carusi, A., & Valsecchi, G. B. 1991, *Icarus*, 94, 98
- Hansen, B. M. S. & Murray, N. 2012, *ApJ*, 751, 158
- Hayashi, C. 1981, Progress of Theoretical Physics Supplement, 70, 35
- Hernández, J., Hartmann, L., Calvet, N., et al. 2008, *ApJ*, 686, 1195
- Hirano, T., Sanchis-Ojeda, R., Takeda, Y., et al. 2012, *ApJ*, 756, 66
- Howard, A. W., Marcy, G. W., Bryson, S. T., et al. 2012, *ApJ Supplement Series*, 201, 15
- Howard, A. W., Marcy, G. W., Johnson, J. A., et al. 2010, *Science*, 330, 653
- Ida, S. & Lin, D. N. C. 2010, *ApJ*, 719, 810
- Ikoma, M. & Hori, Y. 2012, *ApJ*, 753, 66
- Johansen, A., Oishi, J. S., Low, M., et al. 2007, *Nature*, 448, 1022
- Kenyon, S. J. & Bromley, B. C. 2006, *AJ*, 131, 1837
- Kley, W. & Nelson, R. P. 2012, *ARA&A*, 50, 211
- Kokubo, E. & Ida, S. 2000, *Icarus*, 143, 15
- Kramm, U., Nettelmann, N., Fortney, J. J., Neuhäuser, R., & Redmer, R. 2012, *A&A*, 538, A146
- Kramm, U., Nettelmann, N., Redmer, R., & Stevenson, D. J. 2011, *A&A*, 528, A18
- Kuchner, M. J. 2004, *ApJ*, 612, 1147
- Lecar, M., Podolak, M., Sasselov, D., & Chiang, E. 2006, *ApJ*, 640, 1115
- Lee, A. T., Chiang, E., Asay-Davis, X., & Barranco, J. 2010a, *ApJ*, 718, 1367
- Lee, A. T., Chiang, E., Asay-Davis, X., & Barranco, J. 2010b, *ApJ*, 725, 1938
- Lee, M. H. & Peale, S. J. 2002, *ApJ*, 567, 596
- Lissauer, J. J., Fabrycky, D. C., Ford, E. B., et al. 2011a, *Nature*, 470, 53
- Lissauer, J. J., Hubickyj, O., D’Angelo, G., & Bodenheimer, P. 2009, *Icarus*, 199, 338
- Lissauer, J. J., Ragozzine, D., Fabrycky, D. C., et al. 2011b, *ApJ Supplement Series*, 197, 8
- Lithwick, Y. & Wu, Y. 2012, *ApJ Letters*, 756, L11
- Lodders, K. 2003, *ApJ*, 591, 1220
- Lopez, E. D., Fortney, J. J., & Miller, N. K. 2012, ArXiv e-prints
- Lubow, S. H. & D’Angelo, G. 2006, *ApJ*, 641, 526
- Malhotra, R. 1993, *Nature*, 365, 819
- Mardling, R. A. 2007, *MNRAS*, 382, 1768
- Mayor, M., Marmier, M., Lovis, C., et al. 2011, ArXiv e-prints
- Miller-Ricci, E., Seager, S., & Sasselov, D. 2009, *ApJ*, 690, 1056
- Montgomery, R. & Laughlin, G. 2009, *Icarus*, 202, 1
- Murray, C. D. & Dermott, S. F. 2000, *Solar System Dynamics* (Cambridge University Press)
- Murray-Clay, R. A., Chiang, E. I., & Murray, N. 2009, *ApJ*, 693, 23
- Nutzman, P. & Charbonneau, D. 2008, *Publications of the Astronomical Society of the Pacific*, 120, 317
- Perez-Becker, D. & Chiang, E. 2011a, *ApJ*, 735, 8
- Perez-Becker, D. & Chiang, E. 2011b, *ApJ*, 727, 2
- Petrovich, C., Malhotra, R., & Tremaine, S. 2012, ArXiv e-prints
- Rafikov, R. R. 2006, *ApJ*, 648, 666
- Rafikov, R. R. 2012, ArXiv e-prints
- Raymond, S. N., Barnes, R., & Mandell, A. M. 2008, *MNRAS*, 384, 663
- Rein, H. 2012, *MNRAS*, 427, L21
- Ribas, I., Guinan, E. F., Güdel, M., & Audard, M. 2005, *ApJ*, 622, 680
- Ricker, G. R., Latham, D. W., Vanderspek, R. K., et al. 2010, in *Bulletin of the American Astronomical Society*, Vol. 42, American Astronomical Society Meeting Abstracts #215, 450.06
- Rivera, E. J., Laughlin, G., Butler, R. P., et al. 2010, *ApJ*, 719, 890
- Rogers, L. A., Bodenheimer, P., Lissauer, J. J., & Seager, S. 2011, *ApJ*, 738, 59
- Rogers, L. A. & Seager, S. 2010, *ApJ*, 716, 1208
- Schlaufman, K. C., Lin, D. N. C., & Ida, S. 2009, *ApJ*, 691, 1322
- Shi, J.-M. & Chiang, E. 2012, ArXiv e-prints
- Thébaud, P., Marzari, F., & Scholl, H. 2009, *MNRAS*, 393, L21
- Tremaine, S. & Dong, S. 2012, *AJ*, 143, 94
- Wright, J. T., Fakhouri, O., Marcy, G. W., et al. 2011a, *Publications of the Astronomical Society of the Pacific*, 123, 412
- Wright, J. T., Veras, D., Ford, E. B., et al. 2011b, *ApJ*, 730, 93
- Wu, Y. & Goldreich, P. 2002, *ApJ*, 564, 1024
- Wu, Y. & Lithwick, Y. 2011, *ApJ*, 735, 109
- Wu, Y. & Lithwick, Y. 2012, ArXiv e-prints
- Youdin, A. N. 2011, *ApJ*, 742, 38
- Youdin, A. N. & Goodman, J. 2005, *ApJ*, 620, 459
- Zakamska, N. L., Pan, M., & Ford, E. B. 2011, *MNRAS*, 410, 1895